PAPER

Check for updates

Influence of gas molecule adsorption on the mechanical properties of the graphene/aluminum interface

Wei Wang, [ID] [a] Weiwei Xu,[a] Can Cui,[b] Fangfang Xia,[b] Tieqiang Gang*[a] and Lijie Chen*[a]

The graphene/aluminum (Gr/Al) interface plays a critical role in determining the mechanical properties of Gr/Al composites. During fabrication and service, the adsorption of gas molecules at the interface can significantly influence the mechanical properties. In this study, density functional theory (DFT) is employed to simulate the adsorption of H_2, O_2 and CO_2 at the Gr/Al interface and the associated changes in electronic structure and mechanical properties are systematically investigated. The simulation results reveal that O_2 adsorption increases the interface binding energy but reduces the ideal strength, owing to the pronounced resonance peaks formed between O-p orbitals and Al-p\C-p orbitals, which destabilize the interface. H_2 adsorption leads to direct interaction between H_2 molecules and the aluminum matrix, thereby affecting the interface mechanical performance. By contrast, CO_2 adsorption exhibits negligible interaction with the aluminum matrix, resulting in the integrity maintenance of the Gr/Al interface with the highest ideal strength. Further analysis demonstrates that the elastic behavior of the interface is mainly dominated by the aluminum matrix, whereas structural failure originates from the fracture of the graphene structure.

1. Introduction

Graphene-reinforced aluminum matrix composites (Gr/Al) exhibit outstanding properties such as low density, high specific strength and a low coefficient of thermal expansion, which render them promising candidates for applications in advanced engineering fields including aerospace and automotive industries.[1–8] As a high-performance reinforcement phase, graphene can substantially enhance the hardness, strength and wear resistance of aluminum-based composites.[9–15] The mechanical properties of Gr/Al composites are largely governed by the characteristics of the graphene–aluminum interface.[16–18] However, during both fabrication and service, these materials are often exposed to various gaseous environments, where small gas molecules may adsorb at or penetrate the interface region, consequently affecting interfacial stability and mechanical integrity. Due to its high surface activity, graphene readily adsorbs small gas molecules,[19–21] and such adsorption at the interface can further modify the interfacial bonding, electronic structure, and mechanical response of the composite. Recent studies have further demonstrated that environmental gas adsorption can significantly influence the structural stability and surface chemistry of carbon-based materials, highlighting the necessity of understanding gas–solid interactions in

practical service conditions.[22,23] Direct experimental observation of small-molecule adsorption and its impact on the interfacial mechanics remains challenging, primarily due to the limited spatial resolution of current characterization techniques. In contrast, computational simulations offer an effective alternative for probing the atomic-scale structure and mechanical behavior of interfaces.[24–26]

Among these, first-principles calculations based on density functional theory (DFT) have been widely applied to investigate the adsorption characteristics for small molecules on graphene or carbon nanotube surfaces,[27–29] as well as the interfacial properties of graphene/metal (Gr/M) composites.[30–32] Furthermore, first-principles approaches have proven to be powerful tools for elucidating the intrinsic mechanical properties of materials at the microscopic level. The interfacial bonding strength and mechanical performance of composites are highly sensitive to charge distribution, structural stability and local chemical modifications induced by dopants or adsorbed species. Huang *et al.*[30] reported that carbon vacancies and silicon doping can alter the fracture energy and tensile strength of the Gr/Al interface, highlighting the importance of uniform charge distribution for interfacial stability. Polfus *et al.*[33] demonstrated that oxygen atoms in Al–O–C bonds at the alumina/graphene oxide interface yields a binding energy up to 0.8 eV, indicating high structural stability. Similarly, Liu *et al.*[34] revealed that nitrogen (N), boron (B) and co-doping of N–B in the Gr/Al interface disrupt C–C interactions in graphene while

[a]School of Aerospace Engineering, Xiamen University, Xiamen, 361000, China. E-mail: gangtq@xmu.edu.cn; chenlijie@xmu.edu.cn

[b]School of Aeronautics, Chongqing Jiaotong University, Chongqing, 400074, China

enhancing C–Al bonding near the dopant sites, thereby improving interfacial adhesion strength.

In this work, the present study employs first-principles calculations to systematically investigate the adsorption behaviors of H_2, O_2 and CO_2 molecules on the Gr/Al interface and elucidate their effects on the interfacial electronic properties, binding energy and in-plane ideal tensile strength. By examining the electronic and mechanical responses under various adsorption configurations, this study reveals the microscopic mechanisms underlying interfacial strength degradation and provides theoretical guidance for the design and optimization of high-performance graphene/aluminum composites capable of stable operation in compels gaseous environments.

2. Computational methods and models

First-principles calculations based on density functional theory (DFT) are performed to investigate the adsorption behaviors of H_2, O_2 and CO_2 molecules on the graphene/aluminum (Gr/Al) interface, as well as their effects on the electronic properties and ideal tensile strengths of the interface. All simulations are conducted using the Vienna *Ab initio* Simulation Package (VASP).[35] The projector-augmented wave (PAW) pseudopotential method is employed, and the Perdew–Burke–Ernzerhof (PBE) form of the generalized gradient approximation (GGA) is used to describe the exchange-correlation functional. To account for long-range van der Waals interactions inadequately captured by conventional GGA, the DFT-D3 dispersion correction scheme[36–38] is incorporated. The plane-wave energy cutoff is set to 550 eV, and the Brillouin zone is sampled using a $9 \times 9 \times 3$ Monkhorst–Pack k-point mesh, which provides improved numerical stability compared with Γ-point sampling in the vacuum direction. The convergence criteria are set to 10^{-6} eV for the total energy and 10^{-3} eV Å^{-1} for atomic forces. During the tensile simulations, all atomic positions are fully relaxed without any constraints.

The Gr/Al interface models are constructed from six atomic layers of Al(111) and a single layer of Gr(0001). The face-centered cubic (fcc) Al lattice constant is 4.04 Å, corresponding to 2.86 Å for the Al(111) surface, while the lattice constant of Gr(0001) is 2.47 Å. In constructing the interface, the in-plane lattice parameter of the $\sqrt{3} \times \sqrt{3}$ Al(111) substrate is taken as the reference, and the graphene layer is slightly strained (<2%) to achieve commensurability. After the supercell is built, all atomic positions are fully relaxed without imposing any constraints on the atomic coordinates to obtain the energetically stable interface structure. A 15 Å vacuum layer is added along the c-axis to eliminate spurious interactions between periodic images.

Fig. 1(a) and (b) present the side and top views of the pristine Gr/Al interfacial structure, respectively. The 18th Al atom (Al18) is chosen as the adsorption site, and the gas molecules are oriented along the graphene diagonal. This orientation is applied only as the starting configuration; during structural relaxation, no symmetry or rotational constraints are imposed, and all atoms are fully free to adjust their positions and orientations. This consistent initial placement ensures a uniform comparison among different adsorbates without affecting the relaxed adsorption geometries. The adsorption configurations of H_2, O_2 and CO_2 on the Gr/Al interface are denoted as Gr/Al–H_2, Gr/Al–O_2 and Gr/Al–CO_2, respectively, as shown in Fig. 1(c)–(e). In all configurations, the gas molecules are initially
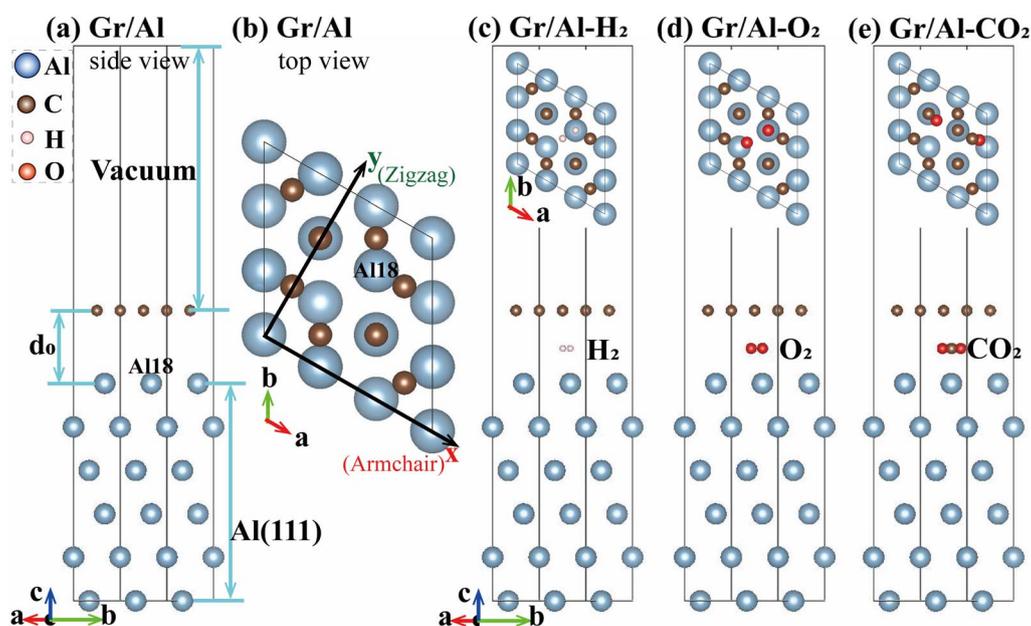

Fig. 1 Side view (a) and top view (b) of the atomic structure of the Gr/Al interface, and schematic representations of the atomic configurations of (c) H_2, (d) O_2 and (e) CO_2 molecules adsorbed on the Gr/Al interface.

positioned at the midpoint between the graphene and aluminum layers along the c-axis, directly above the Al18 atom. The H_2 and O_2 molecules are aligned along the graphene diagonal, while in the CO_2 configuration, the carbon atom is located vertically above Al18, with two oxygen atoms symmetrically distributed along the a-axis.

3. Results and discussion

3.1 Electronic properties

To investigate the effects of gas molecule adsorption on the stability and electronic properties of the Gr/Al interface structure, the adsorption configurations are geometrically optimized, and their charge density differences are analyzed. The initial Gr/Al interface without gas molecule adsorption has lattice constants of $a = b = 4.95$ Å, $c = 29.72$ Å, and angles $\alpha = \beta = 90°$, $\gamma = 120°$. Adsorption of gas molecules at the interface induces noticeable changes in molecular orientation and interfacial spacing.

To optimized atomic configurations and charge density difference plots of H_2, O_2 and CO_2 molecules adsorbed on the Gr/Al interface are shown in Fig. 2. In Fig. 2(a), the Gr/Al–H_2 and Gr/Al–CO_2 systems exhibited significant increases in interlayer spacing after optimization. In the Gr/Al–H_2 structure, the H_2 molecule retains its diagonal orientation relative to graphene, whereas in the Gr/Al–CO_2 structure, the two oxygen atoms

rotated from the initially symmetric alignment along the a-axis to an orientation approximately along the graphene diagonal. This behavior indicates that CO_2 undergoes dissociative adsorption at the interface, as reflected by the bending of the O–C–O angle and the distortion of the C–O bonds. Compared with H_2 and CO_2 adsorption, which only slightly affects the interfacial geometry, adsorption of O_2 molecules causes substantial distortion of the Al substrate layers, with oxygen atoms almost embedding into the Al substrate, as shown in the optimized Gr/Al–O_2 configuration.

The corresponding charge density difference maps further reveal the bonding characteristics among the interfacial atoms. In Fig. 2(b), for the Gr/Al–H_2 and Gr/Al–CO_2 adsorption structures, the electron redistribution between the adsorbed gas molecules and the C or Al atoms in the interface are negligible, indicating a typical physisorption behavior. Consequently, the adsorption of H_2 and CO_2 molecules has a minimal influence on the electronic properties of the interface. In contrast, for the Gr/Al–O_2 structure, adsorption of O_2 induces significant charge transfer at the interface, with evident electron accumulation around the oxygen atoms and electron depletion near the aluminum atoms, leading to the formation of stable Al–O bonds. This redistribution of electrons enhances the interfacial bonding strength and modifies the electronic characteristics of the interface structures.
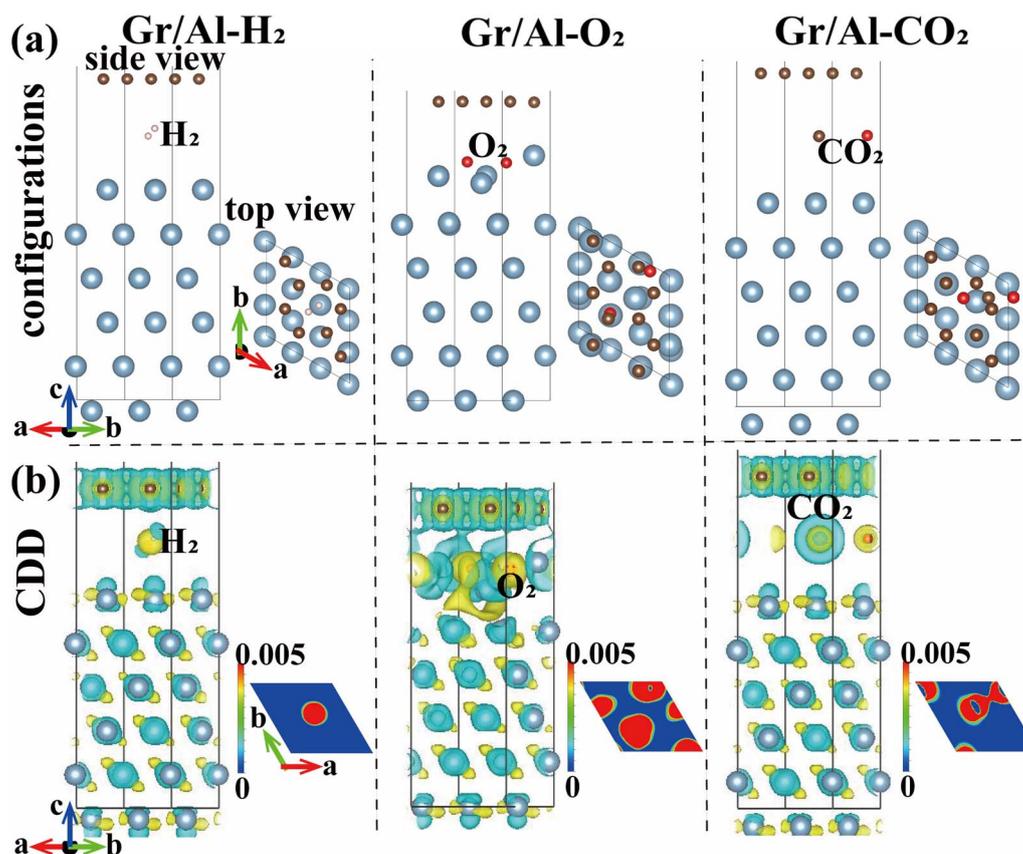

Fig. 2 Optimized (a) atomic configurations and (b) charge density difference (CDD) maps of the Gr/Al interfaces with H_2, O_2 and CO_2 adsorption (iso-surface value: 0.005 e bohr^{-3}; slice taken at the ab plane through the C atom of CO_2).

Table 1 Key physical parameters of the Gr/Al interface adsorption structures

Models	a/Å	d_{Gr-Al}/Å	E_{fermi}/eV	W_f/eV	E_b/eV
Gr/Al–H$_2$	4.95	5.81	2.65	4.23	−4.31
Gr/Al–O$_2$	4.95	3.92	2.96	4.06	−7.79
Gr/Al–CO$_2$	4.95	6.82	2.94	4.23	0.07
Gr/Al	4.95	3.89	2.65	3.91	

Table 1 summarizes the key physical parameters of the Gr/Al interface structures with adsorbed H$_2$, O$_2$, and CO$_2$ molecules. The lattice constant a characterizes the in-plane geometric dimensions of the interface structures within the ab-plane; the interfacial spacing $d_{Gr/Al}$ denotes the average vertical distance along the c-axis between the graphene layer and the aluminum atomic layers; the work function W_f represents the minimum energy required for an electron to escape from the material surface, defined as the difference between the vacuum electrostatic potential and the Fermi level; and the interfacial binding energy E_b serves as a critical indicator for assessing the thermodynamic stability of the interface structure, which is:

$$E_b = E_{Gr/Al-molecule} - (E_{Gr/Al} + E_{molecule}) \qquad (1)$$

where $E_{Gr/Al-molecule}$ is the total energy of the Gr/Al interface structures with an adsorbed gas molecule; $E_{Gr/Al}$ the energy of the Gr/Al interface structures; $E_{molecule}$ the energy of an isolated gas molecule; E_b the interfacial binding energy. A negative value of E_b indicates that the adsorption process is exothermic and leads to a thermodynamically stable interface, whereas a positive value signifies that the adsorption process is endothermic and thermodynamically unfavorable, in which case the molecule tends to desorb rather than form a stable adsorbed state.

Table 1 reveals that the lattice constant a of all three interface adsorption structures remain unchanged at 4.95 Å, indicating that gas adsorption does not induce significant in-plane distortion within the ab-plane. The initial Gr/Al interface without gas adsorption exhibits an interfacial spacing $d_{Gr/Al}$ of 3.89 Å. Upon gas adsorption, the interfacial spacing increase for all threes systems. Among them, the Gr/Al–CO$_2$ structure exhibits the largest interfacial spacing of 6.82 Å, implying that the interface is primarily governed by van der Waals interactions. The Gr/Al–H$_2$ interface shows a moderated interfacial spacing of 5.81 Å, whereas the Gr/Al–O$_2$ structure exhibits the smallest interfacial spacing of 3.92 Å, only a 0.75% increase

compared to the pristine interface, accompanied by notable lattice distortion within the aluminum substrate due to O$_2$ adsorption.

Gas molecule adsorption generally raises the work function (W_f) of the Gr/Al interface, reflecting the influence of adsorbed molecules on surface electron distribution. The work functions of the Gr/Al–H$_2$ and Gr/Al–CO$_2$ systems are both 4.23 eV, representing an 8.74% increase relative to the pristine Gr/Al interface (3.89 eV). In contrast, the Gr/Al–O$_2$ interface exhibits a smaller increase, with a work function of 3.92 eV (0.77% higher). This trend indicates that variations in work function are closely related to electronic redistribution at the interface structures upon molecular adsorption. The adsorption of gas molecules also affects the interfacial binding energy to different extents. Among the three systems, the Gr/Al–O$_2$ structure possesses the lowest binding energy (−7.79 eV), suggesting the strongest and most stable adsorption. The Gr/Al–H$_2$ and Gr/Al–CO$_2$ structures shows binding energies of −4.31 eV and +0.07 eV, respectively, indicating that O$_2$ adsorption on the Gr/Al interface is much more favorable than H$_2$ or CO$_2$ adsorption. The positive binding energy of the Gr/Al–CO$_2$ system suggests that CO$_2$ molecules tend to desorb or dissociation, making this adsorption configuration thermodynamically unstable. These observations indicate that gas-molecule adsorption modulates the electronic properties of the Gr/Al interface in a species-specific manner.

The band structure provides a direct reflection of the electronic state distribution within a material and serves as an intuitive means to reveal the evolution of the electronic states in the Gr/Al interface structure following gas molecule adsorption. It offers insight into changes in electronic characteristics near the Fermi level, bandgap variations and orbital hybridization effects, thereby enabling a deeper understanding of how gas adsorption influences the electronic properties of the Gr/Al interface. The calculated band structures of the three interface adsorption configurations, Gr/Al–H$_2$, Gr/Al–CO$_2$ and Gr/Al–O$_2$ are presented in Fig. 3. By comparing the band structures of these systems, the adsorption characteristics of different gas molecules and their corresponding effects on the interfacial electronic properties are elucidated.

Fig. 3(b) and (d) depict the band structures of the Gr/Al–H$_2$ and Gr/Al–CO$_2$ interface structures, respectively. As previously discussed in the analysis of interfacial parameters, both H$_2$ and CO$_2$ molecules exhibit weak interactions with the Gr/Al interface, indicative of physical adsorption without the formation of
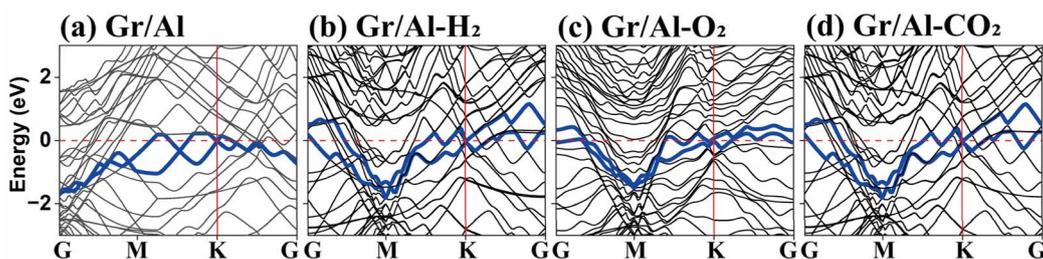
Fig. 3 Band structures of the pristine Gr/Al interface and the interfaces with adsorbed (b) H$_2$, (c) O$_2$ and (d) CO$_2$ molecules.
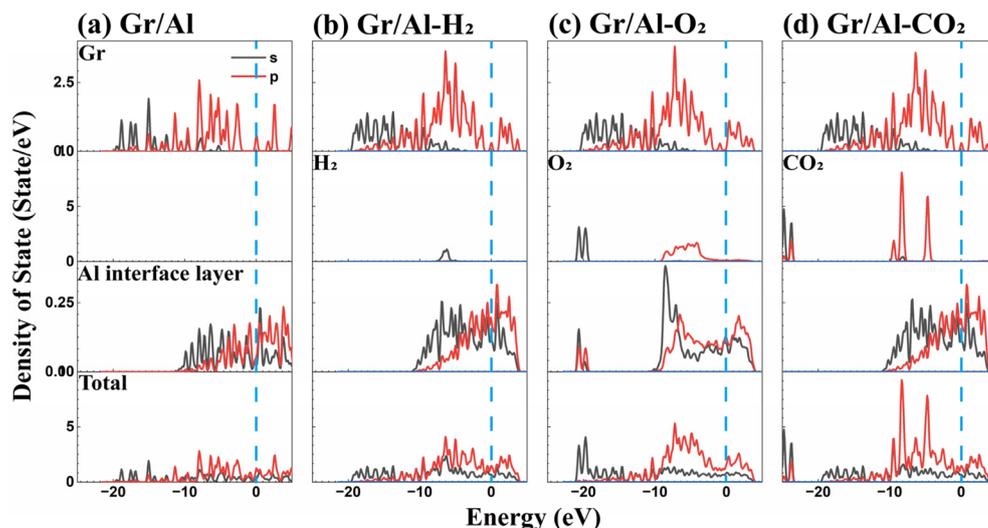
Fig. 4 Density of states of the (a) pristine Gr/Al interface and the interfaces with adsorbed (b) H_2, (c) O_2 and (d) CO_2 molecules.

covalent bonds. This observation is further confirmed by their band structures. The characteristic Dirac cone of graphene remains intact after H_2 and CO_2 adsorption, maintaining a zero-bandgap feature at the K-point. No bandgap opening or new electronic states appear near the Fermi level, indicating that the π-electron network of graphene is essentially unperturbed and that the intrinsic electronic characteristics of the Gr/Al interface remain unaltered by the weak adsorption of H_2 and CO_2 molecules.

In contrast, Fig. 3(c) shows the band structure of the Gr/Al–O_2 interface, where O_2 adsorption induces pronounced modifications. Due to the high electron affinity of the O_2 molecule, it nearly embeds into the Al substrate of the Gr/Al interface, resulting in significant charge transfer and the formation of C–O–Al bonds. Consequently, the intrinsic electronic properties of graphene are strongly perturbed. The band structure reveals that the linear dispersion at the K-point is disrupted, the Dirac cone disappears and the zero-bandgap feature vanishes. A distinct bandgap emerges, indicating that O_2 adsorption not only redistributes charge density across the interface but also triggers orbital hybridization and band structure reconstruction. These changes substantially affecting the electronic

properties of the interface. Accordingly, the electronic behavior of the Gr/Al interfaces exhibits marked molecule-dependent variability.

The density of states (DOS) provides valuable insight into the electronic states distribution of a system and the contributions of individual atomic orbitals. To further investigate the influence of gas molecule adsorption on the electronic properties of the Gr/Al interfaces, the DOS profiles of the three adsorption configurations, Gr/Al–H_2, Gr/Al–CO_2 and Gr/Al–O_2 are calculated and shown in Fig. 4. The plots include the DOS of the graphene layer (Gr), the adsorbed molecules (H_2, O_2 or CO_2), the interfacial Al atomic mono-layer (Al) and the total DOS of the entire interface structures.

In the Gr/Al–H_2 and Gr/Al–CO_2 structures, the electronic states of H_2 and CO_2 molecules are distributed within the energy range of −20 eV to 0 eV. Notably, CO_2 also exhibits a secondary peak at approximately −25 eV. The DOS peaks of H_2 around −8 eV and those of CO_2 near −8 eV and −25 eV, and their DOS peaks show no significant overlap with those of C or Al atoms. This indicates a low degree of orbital hybridization between the adsorbed molecules and the interfacial atoms, suggesting that the adsorption is dominated by van der Waals
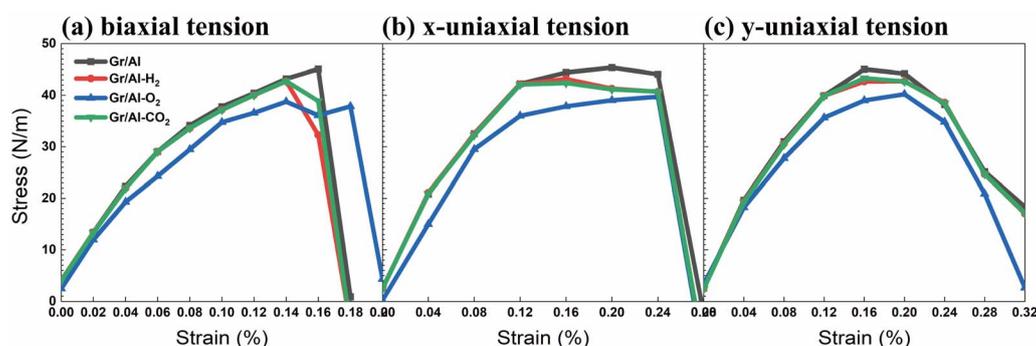

Fig. 5 Stress–strain curves of the pristine Gr/Al, Gr/Al–H_2, Gr/Al–O_2 and Gr/Al–CO_2 interfacial adsorption structures under tensile loading along the (a) xy-, (b) x- and (c) y-directions.

interactions and can be characterized as physical adsorption. Consequently, the intrinsic electronic properties of the Gr/Al interface remain essentially unaltered. In contrast, for the Gr/Al–O$_2$ absorption structure, the DOS of the O$_2$ molecule exhibits a pronounced peak near −20 eV, where the O-s orbital overlaps with the secondary peak of the Al-s orbitals, forming distinct resonance peaks that reflect orbital coupling effects. This orbital hybridization implies that O$_2$ adsorption strengthens interfacial bonding while simultaneously modifying the electronic characteristics of the Gr/Al interface.

3.2 Mechanical properties analysis

The mechanical properties of materials can be characterized by stress–strain curves, from which the ultimate tensile strength, fracture strain and fracture mode can be obtained. These curves also reveal the deformation mechanisms of the interface structures during tensile loading and help elucidate the strengthening or weakening effects induced by molecular adsorption. To evaluate the effect of gas molecule adsorption on the mechanical properties of the Gr/Al interface, ideal in-plane tensile simulations are performed for the three adsorption systems, H$_2$, O$_2$ and CO$_2$ within the *ab*-plane, and compared with the pristine Gr/Al interface, which exhibits an ideal tensile strength of approximately 45 N m^{-1} in all directions. In Fig. 5, the stress–strain curves are obtained for biaxial tension (along

the *xy*-direction), uniaxial tension along the *x*-direction (zigzag direction of graphene) and uniaxial tension along the *y*-direction (armchair direction of graphene).

In Fig. 5 all adsorption systems display brittle fracture behaviors under biaxial and *x*-direction tension, as indicated by the sharp drop in stress after reaching the peak value, while a certain degree of ductile fracture behavior is observed under *y*-direction tension. The Gr/Al–H$_2$ and Gr/Al–CO$_2$ structures, both of which maintain relatively good interfacial integrity, exhibit similar stress–strain profiles across all directions. Quantitative analysis of the three adsorption systems reveals that under biaxial tension, the ideal tensile strengths of the Gr/Al–H$_2$, Gr/Al–O$_2$ and Gr/Al–CO$_2$ interfaces are 42.72 N m^{-1} ($\varepsilon = 0.14$), 38.76 N m^{-1} ($\varepsilon = 0.14$) and 42.74 N m^{-1} ($\varepsilon = 0.14$), respectively, with fracture strains of 0.18, 0.20 and 0.18. Under *x*-direction tension, the strengths are 43.16 N m^{-1} ($\varepsilon = 0.16$), 39.72 N m^{-1} ($\varepsilon = 0.24$) and 42.37 N m^{-1} ($\varepsilon = 0.16$), all with a fracture strain of 0.28. Under *y*-direction tension, the ideal strengths are 42.71 N m^{-1} ($\varepsilon = 0.20$), 40.22 N m^{-1} ($\varepsilon = 0.20$) and 43.32 N m^{-1} ($\varepsilon = 0.16$), with fracture strains of 0.32 in each case.

Therefore, Gr/Al–CO$_2$ adsorption structure exhibits the highest calculated mechanical performance, with slightly higher ideal strength and fracture strain than the Gr/Al–H$_2$ interface. It should be noted, however, that the adsorption of CO$_2$ on Gr/Al is endothermic and thermodynamically unlikely to
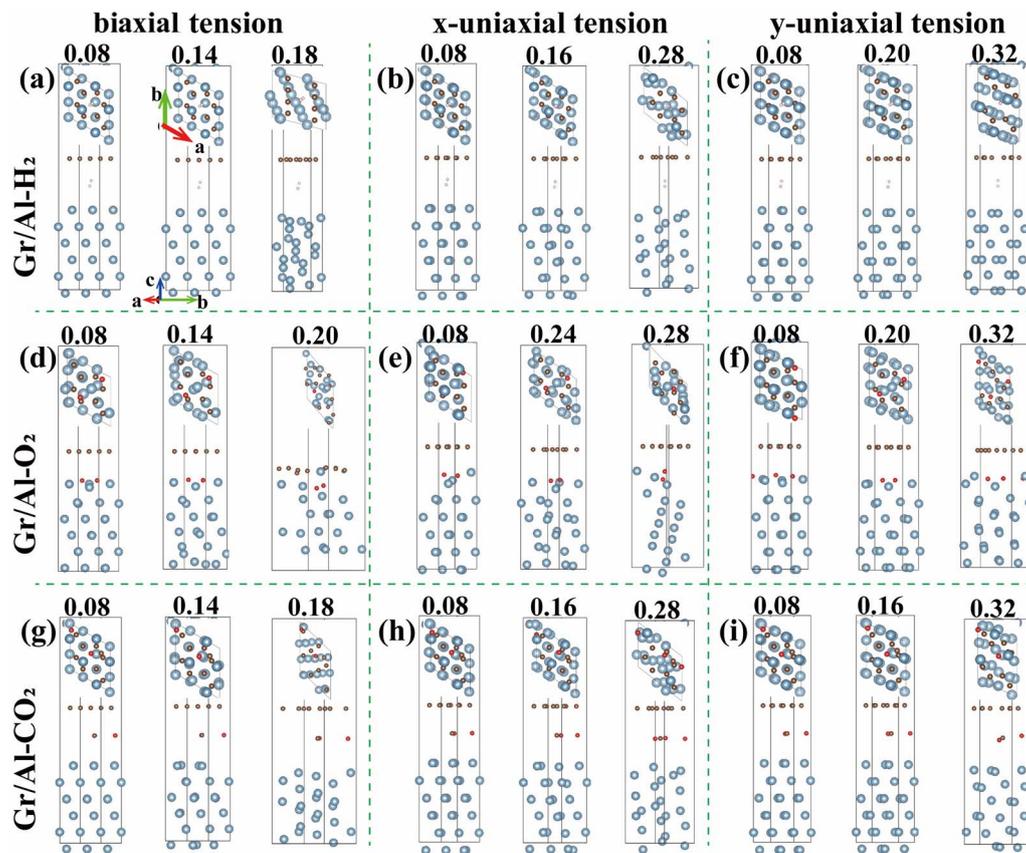

Fig. 6 Atomic configurations of the (a)–(c) Gr/Al–H$_2$, (d)–(f) Gr/Al–O$_2$ and (g)–(i) Gr/Al–CO$_2$ interfacial adsorption structures under tensile loading along the *xy*-, *x*- and *y*-directions.

occur spontaneously; thus, this configuration represents an idealized model. Nevertheless, this indicates that the physical adsorption of CO_2 molecules has the weakest influence on the mechanical integrity of the interface. In contrast, H_2 adsorption maintains a balance between interfacial integrity and tensile strength. The Gr/Al–O_2 interface exhibits the lowest ideal strength under tension in all directions, indicating that enhances interfacial bonding strength by disrupting the graphene lattice leads to a deterioration in the mechanical performance of the interface.

3.3 Strengthening mechanism analysis

3.3.1 Atomic-scale deformation behavior under tensile loading. To elucidate the deformation mechanisms of the interfacial adsorption structures at the atomic scale and to understand of gas molecule adsorption on their stability and mechanical performance, Fig. 6 presents the Gr/Al–H_2, Gr/Al–O_2 and Gr/Al–CO_2 interfaces under xy-, x- and y-directions tension, showing three stages: elastic ($\varepsilon = 0.08$), ultimate strength and fracture.

In the Gr/Al–H_2 system (Fig. 6(a)–(c)), two hydrogen atoms remain symmetrically distributed at the center of the interface along the diagonal direction of graphene. Elastic deformation is mainly resisted by the Al substrate, where stress concentrations near the aluminum layer of the interface. At $\varepsilon = 0.14$ (ideal strength), Al substrate becomes disordered, while the graphene hexagonal lattice remains relatively intact. At $\varepsilon = 0.18$, the graphene hexagonal rings are severely destroyed, and the Al atoms become fully disordered, resulting in interfacial failure. Under x- and y-directions tension, the H_2 molecule does not chemically interact with either Al or C atoms. Elastic deformation occurs *via* Al layers displacement, and fracture is dominated by C–C bonds breaking. These results indicate that H_2 adsorption does not disrupt the structural stability of the interface, thereby contributing positively to the mechanical performance of the Gr/Al structures.

For the Gr/Al–O_2 interface (Fig. 6(d)–(f)), O_2 molecule exhibits strong interaction with the Gr/Al interface, as the O atoms embed into the Al substrate. Elastic stage deformation causes mild Al disorder and C–C distortion. At ultimate strength, the graphene rings are significantly distorted, and the cooperative interaction among Al, O and C atoms at the interface is enhanced. Upon fracture, the graphene lattice is completely destroyed, and the interfacial spacing nearly vanishes, indicating the formation of a strong interaction region among Al, O and C atoms. This demonstrates that O_2 adsorption increases binding energy but destabilizes the interface, reducing tensile strength.

In the Gr/Al–CO_2 system (Fig. 6(g)–(i)), adsorption behavior of CO_2 is similar to that of H_2, characterized by weak interaction
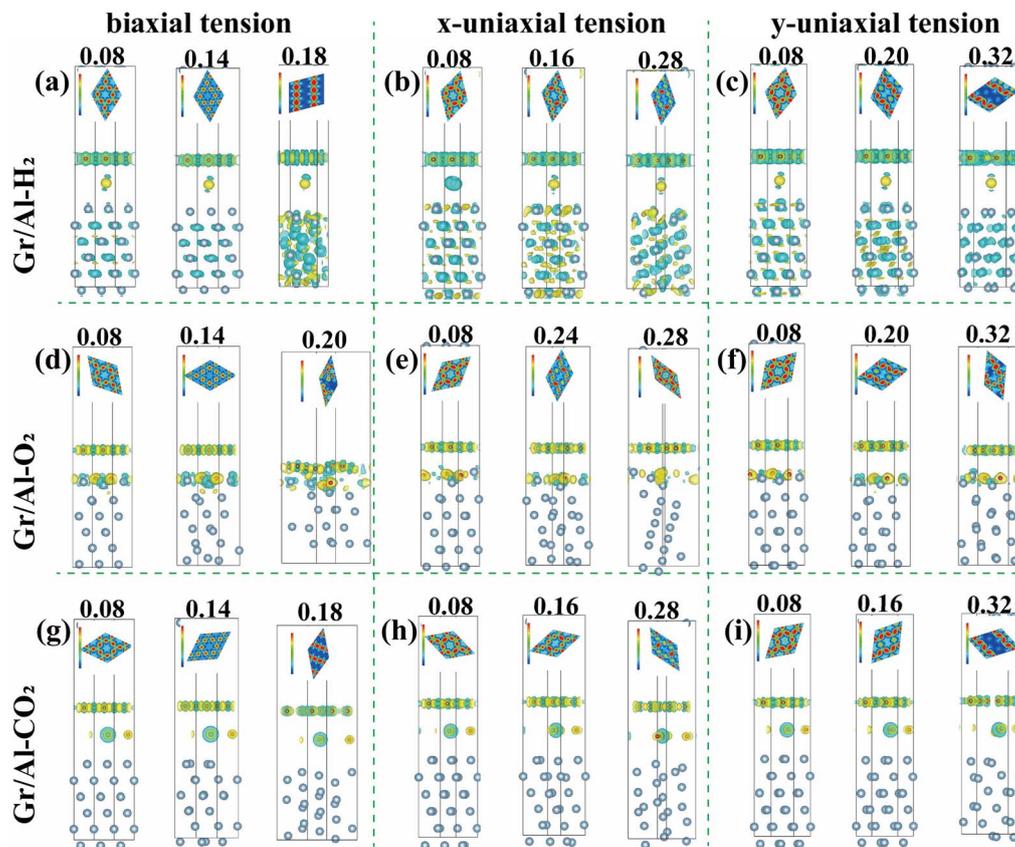

Fig. 7 Charge density difference maps of the (a)−(c) Gr/Al−H_2, (d)−(f) Gr/Al−O_2 and (g)−(i) Gr/Al−CO_2 interfacial adsorption structures under tensile loading along the xy-, x- and y-directions.

with the interface. In the elastic stage, only slight displacements occur in the Al atomic layer, and the interface remains largely intact. At ultimate strength, the CO_2 molecule dissociates, breaking the linear O–C–O configuration: one O atom moves away from the central C atom, while the other forms a weak interaction with a C atom in the graphene layer. During fracture, the graphene structure becomes significantly damaged. Partial molecular reconstruction minimally affects interfacial distortion, resulting in the highest mechanical performance among the three adsorption systems.

Overall, tensile deformation is dominated by Al substrate distortion, while fracture originates from graphene failure. Strong O_2-interface coupling destabilizes both electronic and mechanical properties, whereas H_2 and CO_2 maintain interfacial stability and superior mechanical performance.

3.3.2 Electronic redistribution during tensile deformation. Charge density difference (CDD) maps reveal how gas adsorption modifies the electronic properties of the Gr/Al interface under tensile deformation. Fig. 7 shows the CDD of Gr/Al–H_2, Gr/Al–O_2 and Gr/Al–CO_2 interface along xy-, x-, and y-directions, corresponding to the atomic configurations in Fig. 6. The isosurface value is set to 0.005 e bohr^{-3}, with cross-sectional slices parallel to the ab-plane of graphene. The yellow regions indicate electron accumulation, and the blue regions electron depletion. Analyzing of charge redistribution identifies the direction of charge transfer and bonding characteristics.

In the Gr/Al–H_2 structure, electron accumulation occurs around the H atoms, accompanied by electron depletion near the Al and C atoms. This indicates that electrons transfer from Al and C atoms to H atoms. The redistribution is delocalized,

with no strong covalent bonds forming, confirming van der Waals adsorption. H_2 adsorption exerts only a minor influence on the electronic properties of the interface.

The Gr/Al–O_2 interface exhibits pronounced charge rearrangement, with accumulation near O and depletion near Al atoms. Electrons migrate from Al to O atoms, leading to local displacement and distortion of Al atoms. Simultaneous accumulation near C atoms indicates disruption of graphene π-bonds and weakened C–C bonds, destabilizing the interface and reducing tensile strength.

For the Gr/Al–CO_2 structure, the C atom in the CO_2 molecule loss electrons, while both O atoms show electron enrichment, indicating charge polarization within the molecule upon adsorption. Electron accumulation near graphene C atoms slightly weakens σ-band hybridization, modestly affecting mechanical integrity.

As strain increases, C atoms in all systems undergo continuous electronic redistribution. At fracture, the electron density around the C atoms decreases significantly, the degree of orbital hybridization is further reduced, and the graphene lattice becomes severely damaged, leading ultimately to and interfacial failure. These results demonstrate that gas molecules adsorption regulates charge transfer and redistribution, which in turn dictates the mechanical response of the interface.

3.3.3 Orbital hybridization as the determinant of strength degradation. Density of states (DOS) analysis reveals how orbital hybridization governs interfacial mechanical properties during tensile deformation. Fig. 8 presents the DOS of the Gr/Al–H_2, Gr/Al–O_2, and Gr/Al–CO_2 interfaces at their ultimate tensile strengths along xy-, x- and y-directions. Graphene (Gr),
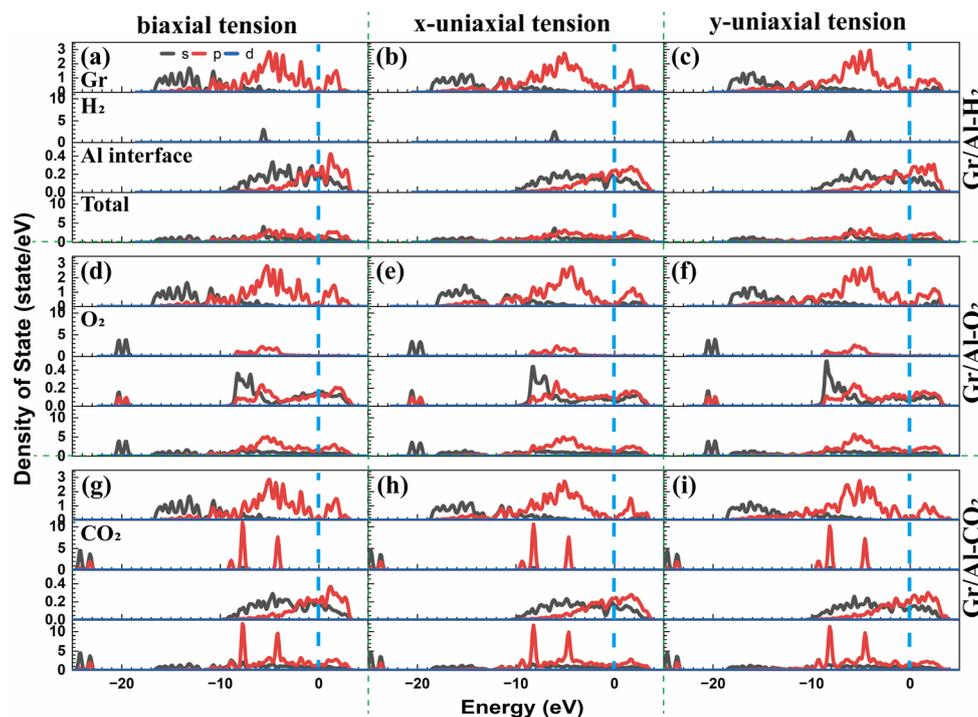

Fig. 8 Density of states of the (a)–(c) Gr/Al–H_2, (d)–(f) Gr/Al–O_2 and (g)–(i) Gr/Al–CO_2 interfacial adsorption structures under tensile loading along the xy-, x- and y-directions.

adsorbed molecules (H_2, O_2 and CO_2), interfacial Al layer (Al interface) and the total DOS (total) are presented to analyze the influences of gas adsorption on the electronic properties.

For the Gr/Al–H_2 interface, s orbitals of H atoms and Al exhibit a weak resonance peak around −5 eV, suggesting slight orbital hybridization. This weak interaction enhances the interfacial binding energy without disturbing the electronic structures, and no H–C orbitals coupling occurs, preserving physisorption and mechanical stability.

For the Gr/Al–O_2 interface, pronounced resonance peaks appear near −5 eV due to the hybridization between the O-p orbital and C-p/Al-p orbitals, indicating much stronger orbital coupling compared with H_2 adsorption. This hybridization increases binding energy but induces structural distortion and stress concentration, reducing ideal tensile strength.

For the Gr/Al–CO_2 structure, a DOS peak appears near −5 eV for CO_2, but no resonance with Al or C orbitals is observed, indicating negligible hybridization. Therefore, CO_2 adsorption minimally affects electronic structures, maintaining interfacial stability and yielding the highest ideal strength.

Despite the potential for experimental probing *via* AFM force-spectroscopy or nanoindentation, mechanical performance of the interfacial adsorption structures depends not only on the interaction strength between gas adsorbed molecules and interfacial atoms but also on the structural integrity and electronic characteristics of both graphene and the aluminum substrate. O_2 adsorption induces strong orbital hybridization that disrupts structural integrity and reduces the ideal strength, whereas H_2 and CO_2 adsorption cause significant hybridization, preserving structural stability and superior mechanical performance. The influence of gas adsorption on the mechanical properties is closely correlated with orbital hybridization: weaker hybridization results in smaller structural damage and better mechanical performance.

4. Conclusions

Based on first-principles calculations, this work investigates the effects of H_2, O_2 and CO_2 molecules adsorption on the electronic characteristics and in-plane mechanical performance of the Gr/Al interface. The main conclusions are:

(1) Among the three adsorption systems, the O_2-adsorbed Gr/Al interface exhibits the highest binding energy and the smallest interfacial spacing. Significant orbital hybridization and charge transfer occur during adsorption, which disrupt the zero-band-gap characteristic of graphene and induce local structural reconstruction. In contrast, H_2 and CO_2 molecules adsorbed at the intermediate region of the Gr/Al interface exhibit only weakly interactions with the substrate, without forming evident covalent bonds. The band structure analysis indicates that the intrinsic electronic properties of graphene are well preserved, leading to higher structural stability.

(2) In-plane tensile simulations along the *xy*-, *x*- and *y*-directions of the Gr(0001) plane are conducted and the calculated ideal strengths of the three adsorption structures follow the order Gr/Al–CO_2 > Gr/Al–H_2 > Gr/Al–O_2. The Gr/Al–CO_2 structure shows the highest ideal strengths of 42.74 N m^{-1},

42.37 N m^{-1} and 43.32 N m^{-1} along the *xy*-, *x*- and *y*-directions, respectively. By comparison, the Gr/Al–O_2 structure exhibits the lowest strength in all directions, indicating that strong interfacial interactions enhance the binding energy but compromise mechanical performance.

(3) During tensile deformation, the elastic response of the interface is primarily dominated by the aluminum matrix, while the graphene reinforcement contributes to structural stability. The overall failure of the interface is attributed to the fracture of the graphene layer. For the Gr/Al–O_2 interface, strong interactions between O_2 molecules and Al atoms occur during elastic deformation, resulting in atomic rearrangement in the Al substrate and slight distortion of the C–C bonds near the O atoms. At fracture, the graphene layer is completely destroyed, the interfacial spacing approaches zero, and the Al–O–C coupling is significantly enhanced, leading to total interfacial instability. For the Gr/Al–H_2 and Gr/Al–CO_2 structures, the interaction between the adsorbed molecules and the interface remains weak during deformation. Only minor atomic displacements occur in the Al substrate, and the interface structure maintains high structural integrity. Upon fracture, the adsorbed molecules dissociate, accompanied by substantial graphene damage.

(4) The orbital coupling between interfacial atoms is identified as the key factor governing mechanical properties. In the Gr/Al–O_2 interface, pronounced hybridization among the p orbitals of O, Al and C atoms weakens the in-plane C–C covalent bonds, reducing the mechanical strength. In the Gr/Al–H_2 system, resonance occurs between the H-s and Al-s orbitals, exerting a slightly influence on interfacial strength. In contrast, in the Gr/Al–CO_2 interface, neither C nor O atoms from the CO_2 molecule show significant orbital hybridization with the interfacial Al or C atoms, thus maintaining the structural integrity and yielding the highest ideal strength.

In summary, gas adsorption influences both the electronic and mechanical properties of the Gr/Al interface. Weak physisorption is more favorable for preserving interface stability and ideal strength. This study provides theoretical guidance for understanding and optimizing the performance of graphene/metal composites under complex gaseous environments.

Author contributions

Conceptualization, W. W., W. W. X., T. Q. G. and L. J. C.; methodology, W. W., W. W. X., T. Q. G. and L. J. C.; software, W. W., W. W. X., T. Q. G. and L. J. C.; validation, W. W., W. W. X., T. Q. G. and L. J. C.; formal analysis, W. W., W. W. X., T. Q. G. and L. J. C.; investigation, W. W., W. W. X., C. C., T. Q. G. and L. J. C.; resources, W. W., T. Q. G. and L. J. C.; data curation, W. W., W. W. X., T. Q. G. and L. J. C.; writing—original draft preparation, W. W., W. W. X., T. Q. G. and L. J. C.; writing—review and editing, W. W., W. W. X., T. Q. G. and L. J. C.; visualization, W. W., W. W. X., T. Q. G. and L. J. C.; supervision, W. W., W. W. X., C. C., F. F. X., T. Q. G. and L. J. C.; project administration, W. W., W. W. X., T. Q. G. and L. J. C.; funding acquisition, W. W. X., F. F. X. and L. J. C. All authors

have read and agreed to the published version of the manuscript.

Conflicts of interest

The authors declare no conflicts of interest.

Data availability

All data generated or analyzed during this study are included in this published article. Additional data are available from the corresponding author upon reasonable request.

Acknowledgements

References

1 W. Zhou, Y. Fan, X. Feng, K. Kikuchi, N. Nomura and A. Kawasaki, Creation of individual few-layer graphene incorporated in an aluminum matrix, *Composites, Part A*, 2018, **112**, 168–177, DOI: 10.1016/j.compositesa.2018.06.008.

2 Z. W. Zhang, Z. Y. Liu, B. L. Xiao, D. R. Ni and Z. Y. Ma, High efficiency dispersal and strengthening of graphene reinforced aluminum alloy composites fabricated by powder metallurgy combined with friction stir processing, *Carbon*, 2018, **135**, 215–223, DOI: 10.1016/j.carbon.2018.04.029.

3 R. Guan, Y. Wang, S. Zheng, N. Su, Z. Ji, Z. Liu, Y. An and B. Chen, Fabrication of aluminum matrix composites reinforced with Ni-coated graphene nanosheets, *Mater. Sci. Eng., A*, 2019, **754**, 437–446, DOI: 10.1016/j.msea.2019.03.068.

4 G. Wu, Z. Yu, L. Jiang, C. Zhou, G. Deng, X. Deng and Y. Xiao, A novel method for preparing graphene nanosheets/Al composites by accumulative extrusion-bonding process, *Carbon*, 2019, **152**, 932–945, DOI: 10.1016/j.carbon.2019.06.077.

5 Y. Zhang and X. Li, Bioinspired, Graphene/Al2O3 Doubly Reinforced Aluminum Composites with High Strength and Toughness, *Nano Lett.*, 2017, **17**(11), 6907–6915, DOI: 10.1021/acs.nanolett.7b03308.

6 Y. Xie, X. Meng, Y. Huang, J. Li and J. Cao, Deformation-driven metallurgy of graphene nanoplatelets reinforced aluminum composite for the balance between strength and ductility, *Composites, Part B*, 2019, **177**, 107413, DOI: 10.1016/j.compositesb.2019.107413.

7 Z. Yu, W. Yang, C. Zhou, N. Zhang, Z. Chao, H. liu, Y. Cao, Y. Sun, P. Shao and G. Wu, Effect of ball milling time on graphene nanosheets reinforced Al6063 composite fabricated by pressure infiltration method, *Carbon*, 2019, **141**, 25–39, DOI: 10.1016/j.carbon.2018.09.041.

8 J. Jayaseelan, A. Pazhani, A. X. Michael, J. Paulchamy, A. Batako and P. K. Hosamane Guruswamy, Characterization Studies on Graphene-Aluminium Nano Composites for Aerospace Launch Vehicle External Fuel Tank Structural Application, *Materials*, 2022, **15**(17), 5907, DOI: 10.3390/ma15175907.

9 H. M. I. Jaim, R. A. Isaacs, S. N. Rashkeev, M. Kuklja, D. P. Cole, M. C. LeMieux, I. Jasiuk, S. Nilufar and L. G. Salamanca-Riba, Sp2 carbon embedded in Al-6061 and Al-7075 alloys in the form of crystalline graphene nanoribbons, *Carbon*, 2016, **107**, 56–66, DOI: 10.1016/j.carbon.2016.05.053.

10 S. Feng, Q. Guo, Z. Li, G. Fan, Z. Li, D.-B. Xiong, Y. Su, Z. Tan, J. Zhang and D. Zhang, Strengthening and toughening mechanisms in graphene-Al nanolaminated composite micro-pillars, *Acta Mater.*, 2017, **125**, 98–108, DOI: 10.1016/j.actamat.2016.11.043.

11 S. E. Shin, H. J. Choi, J. H. Shin and D. H. Bae, Strengthening behavior of few-layered graphene/aluminum composites, *Carbon*, 2015, **82**, 143–151, DOI: 10.1016/j.carbon.2014.10.044.

12 G. Li and B. Xiong, Effects of graphene content on microstructures and tensile property of graphene-nanosheets/aluminum composites, *J. Alloys Compd.*, 2017, **697**, 31–36, DOI: 10.1016/j.jallcom.2016.12.147.

13 Y. Huang, Q. Ouyang, D. Zhang, J. Zhu, R. Li and H. Yu, Carbon Materials Reinforced Aluminum Composites: A Review, *Acta Metall. Sin.*, 2014, **27**(5), 775–786, DOI: 10.1007/s40195-014-0160-1.

14 Y. Hu, Q. Guo, L. Zhao, Z. Li, *et al.*, Correlating micro-pillar compression behavior with bulk mechanical properties: Nanolaminated graphene-Al composite as a case study, *Scr. Mater.*, 2018, **146**, 236–240, DOI: 10.1016/j.scriptamat.2017.12.004.

15 N. Seyed Pourmand and H. Asgharzadeh, Aluminum Matrix Composites Reinforced with Graphene: A Review on Production, Microstructure, and Properties, *Crit. Rev. Solid State Mater. Sci.*, 2019, **45**(4), 289–337, DOI: 10.1080/10408436.2019.1632792.

16 M. M. El-Sayed Seleman, M. M. Z. Ahmed and S. Ataya, Microstructure and mechanical properties of hot extruded 6016 aluminum alloy/graphite composites, *J. Mater. Sci. Technol.*, 2018, **34**(9), 1580–1591, DOI: 10.1016/j.jmst.2018.03.004.

17 M. Li, H. Gao, J. Liang, S. Gu, W. You, D. Shu, J. Wang and B. Sun, Microstructure evolution and properties of graphene nanoplatelets reinforced aluminum matrix composites, *Mater. Charact.*, 2018, **140**, 172–178, DOI: 10.1016/j.matchar.2018.04.007.

18 B. Ju, W. Yang, P. Shao, M. Hussain, Q. Zhang, Z. Xiu, X. Hou, J. Qiao and G. Wu, Effect of interfacial microstructure on the mechanical properties of GNPs/Al composites, *Carbon*, 2020, **162**, 346–355, DOI: 10.1016/j.carbon.2020.02.069.

19 Q. Su, S. Pang, V. Alijani, C. Li, X. Feng and K. Müllen, Composites of Graphene with Large Aromatic Molecules,

Adv. Mater., 2009, **21**(31), 3191–3195, DOI: 10.1002/adma.200803808.

20 L. Kong, A. Enders, T. S. Rahman and P. A. Dowben, Molecular adsorption on graphene, *J. Phys.: Condens. Matter*, 2014, **26**(44), 443001, DOI: 10.1088/0953-8984/26/44/443001.

21 M. Chi and Y.-P. Zhao, Adsorption of formaldehyde molecule on the intrinsic and Al-doped graphene: A first principle study, *Comput. Mater. Sci.*, 2009, **46**(4), 1085–1090, DOI: 10.1016/j.commatsci.2009.05.017.

22 X. Shi, L. Gao, E. Alzahrani, J. Hong, A. K. Alanazi, *et al.*, High adsorption performance for trace lead (II) cation from sewage by Fe/Cu metal organic nanosheets modified with terephthalic acid, *Chemosphere*, 2023, **330**, 138637, DOI: 10.1016/j.chemosphere.2023.138637.

23 M. Zheng, J. Ren, C. Wang, *et al.*, Magnetite@poly(p-phenylenediamine) core–shell composite modified with salicylaldehyde for adsorption and separation of Mn (VII) from polluted water, *J. Nanostruct. Chem.*, 2022, **12**(6), 1155–1168, DOI: 10.1007/s40097-022-00510-4.

24 J. Zhou, J. Shen, W. Yue, Y. Liu and Z. Chen, Molecular dynamics simulation of reinforcement mechanism of graphene/aluminum composites and microstructure evolution, *J. Mater. Res. Technol.*, 2023, **23**, 2147–2159, DOI: 10.1016/j.jmrt.2023.01.161.

25 M. Li and X.-W. Lei, Molecular dynamics studies on mechanical properties and deformation mechanism of graphene/aluminum composites, *Comput. Mater. Sci.*, 2022, **211**, 111487, DOI: 10.1016/j.commatsci.2022.111487.

26 X.-N. Hao and X. Liu, Molecular dynamics study on microscale residual stress of graphene/aluminum nanocomposites by selective laser sintering, *Rare Met.*, 2022, **41**(11), 3677–3683, DOI: 10.1007/s12598-022-02079-x.

27 X. Li, J. Feng, E. Wang, S. Meng, J. Klimeš and A. Michaelides, Influence of water on the electronic structure of metal-supported graphene: Insights from van der Waals density functional theory, *Phys. Rev. B*, 2012, **85**(8), 085425, DOI: 10.1103/PhysRevB.85.085425.

28 W. L. Yim, O. Byl, J. T. Yates Jr and J. K. Johnson, Vibrational behavior of adsorbed CO2 on single-walled carbon nanotubes, *J. Chem. Phys.*, 2004, **120**(11), 5377–5386, DOI: 10.1063/1.1648017.

29 A. S. Rad, Al-doped graphene as a new nanostructure adsorbent for some halomethane compounds: DFT calculations, *Surf. Sci.*, 2016, **645**, 6–12, DOI: 10.1016/j.susc.2015.10.036.

30 J. Huang, Y. Liu, Z. Lai, J. Hu, F. Zhou and J. Zhu, A systematic study of interface properties and fracture behavior of graphene/aluminum: Insights from a first-principles study, *Vacuum*, 2022, **204**, 111346, DOI: 10.1016/j.vacuum.2022.111346.

31 Q. Guo, Y. Dedkov and E. Voloshina, Intercalation of Mn in graphene/Cu(111) interface: insights to the electronic and magnetic properties from theory, *Sci. Rep.*, 2020, **10**(1), 21684, DOI: 10.1038/s41598-020-78583-w.

32 X. Zhang and S. Wang, Interfacial Strengthening of Graphene/Aluminum Composites through Point Defects: A First-Principles Study, *Nanomaterials*, 2021, **11**(3), 738, DOI: 10.3390/nano11030738.

33 J. M. Polfus, O. M. Løvvik, P. M. Rørvik and R. Bredesen, Nanocomposites of few-layer graphene oxide and alumina by density functional theory calculations, *J. Eur. Ceram. Soc.*, 2016, **36**(3), 719–724, DOI: 10.1016/j.jeurceramsoc.2015.11.009.

34 P. Liu, J. Xie, A. Wang, D. Ma and Z. Mao, First-principles prediction of enhancing graphene/Al interface bonding strength by graphene doping strategy, *Appl. Surf. Sci.*, 2020, **517**, 146040, DOI: 10.1016/j.apsusc.2020.146040.

35 G. Kresse and J. Hafner, Ab initio molecular dynamics for liquid metals, *Phys. Rev. B:Condens. Matter Mater. Phys.*, 1993, **47**(1), 558–561, DOI: 10.1103/physrevb.47.558.

36 I. Hamada and M. Otani, Comparative van der Waals density-functional study of graphene on metal surfaces, *Phys. Rev. B*, 2010, **82**(15), 153412, DOI: 10.1103/PhysRevB.82.153412.

37 J. Ma, A. Michaelides, D. Alfè, L. Schimka, G. Kresse and E. Wang, Adsorption and diffusion of water on graphene from first principles, *Phys. Rev. B*, 2011, **84**(3), 033402, DOI: 10.1103/PhysRevB.84.033402.

38 T. Schwabe and S. Grimme, Double-hybrid density functionals with long-range dispersion corrections: higher accuracy and extended applicability, *Phys. Chem. Chem. Phys.*, 2007, **9**(26), 3397–3406, DOI: 10.1039/b704725h.